SAND2008-2088C

Practical aspects of contouring using ESPI/DSPI

Phillip L. Reu and Bruce D. Hansche
Sandia National Laboratories, PO Box 5800, Albuquerque, New Mexico 87185

Abstract

Moiré contouring can be implemented by illuminating the object with coherent light from two closely spaced point sources—the so-called “two point” method. This method can be implemented using digital speckle pattern interferometry techniques (DSPI) by illuminating the object with a single point source that is moved between datasets. We briefly present the algorithm used and some inherent implicit and explicit assumptions in using the technique. One of the assumptions is that the object remains stationary between datasets. If violated, this quite strong assumption will create hundreds of microns of error from fractions of a micron of object motion. We present simulations and experiments demonstrating these sensitivities and two techniques to compensate for object motion during data acquisition.

1. Introduction

The use of optical techniques for surface topography measurement, or “contouring”, has been studied extensively. The advantages are fairly obvious: non-contact and wide-field measurements can be made on delicate objects with sizes ranging from micro to huge, by applying the appropriate optical configuration. One technique that dominates this field is geometric moiré, which relies on a grid or grating projected on the object. The resulting image of this grid is a function of the surface shape. It can be analyzed directly, using phase stepping techniques, or compared with a reference grating, in true moiré fashion [1,2]. One way to generate a projected grating is by illuminating the object with coherent light from two closely spaced point sources—the so-called “two-point” method. It is important to realize that in all of the projected grid techniques, the surface topography information is carried by the image *intensity*, even when coherent light is used to produce the grid rather than a projected grid.

Our implementation was driven by the need to accurately measure the deformation of an object—which suggested using electronic/digital speckle pattern interferometry (ESPI or DSPI). A secondary requirement was to measure the preliminary shape of the object. Rather than use two different techniques, it was decided to use the same equipment for both measurements. Several authors have pointed out that ESPI or holographic techniques can be used to measure surface contour. Thalman and Dandliker [1] review various techniques: The two-wavelength technique generates contour fringes with a contour interval relative to $\Delta\lambda$. It can be experimentally difficult to implement, requiring either a tunable laser with slight wavelength variation, or immersion of the object in media with different index of refraction. Other authors implement a “two-source illumination” to generate two closely spaced illumination points *sequentially* with two separate ESPI exposures, which is closely related to the two-point grid projection technique mentioned previously. Joenathan, *et al* [2] rotate the object between ESPI exposures, which is equivalent to moving two illumination beams between exposures. Rodriguez-Vera *et al* [3] analyze contour fringe generation by motion of two illumination beams. Wang, *et al* [4,5] analyze fringe generation by motion of a single illumination point, and suggest the convenience of combining such a contour measurement with ESPI deformation measurements. The papers by Wang, *et al* were our original inspiration for this work, and our notation will in part follow theirs.

All of the two-source methods mentioned above make some assumptions to simplify the analysis process—many of these are implicit. One of the assumptions is that *the object does not move between ESPI exposures made for contouring*. This turns out to be a fairly strong assumption, and in our particular case was a condition impossible to realize. We therefore describe some possible solutions to the problem of object motion during ESPI based two-point contouring.

2. Experimental Configuration

Figure 1 shows the experimental configuration of a standard out-of-plane ESPI configuration. A beam splitter is placed between the lens and the camera sensor to allow the insertion of a reference beam with the object beam launched from the fiber off to the side. Phase shifting is accomplished via a fiber stretcher on the reference leg used with a Carré algorithm to calculate the phase. The object beam is mounted on a stepper motor to move the beam a known amount for creating the two-illumination configuration required for contouring. As ESPI is well understood, no more will be said regarding this aspect other than to note that in this configuration, nearly identical hardware and software can be used for *both* deformation and contouring measurements.

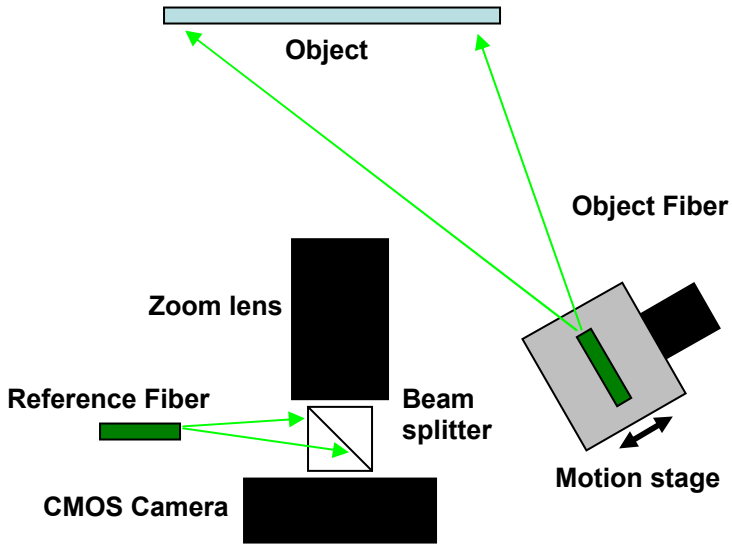

Figure 1. ESPI contouring and out-of-plane deformation measurement setup.

Figure 2 shows simplified diagrams of the experimental contouring geometry for both the case without object motion on the left and with object motion on the right. The illumination source S is assumed to lie in the Y = 0 plane. Between exposures, the illumination source is translated by vector **d** with components (u,w). In general, the object point P might move between exposures by vector **δ.** Vector **k** is the ESPI sensitivity vector.

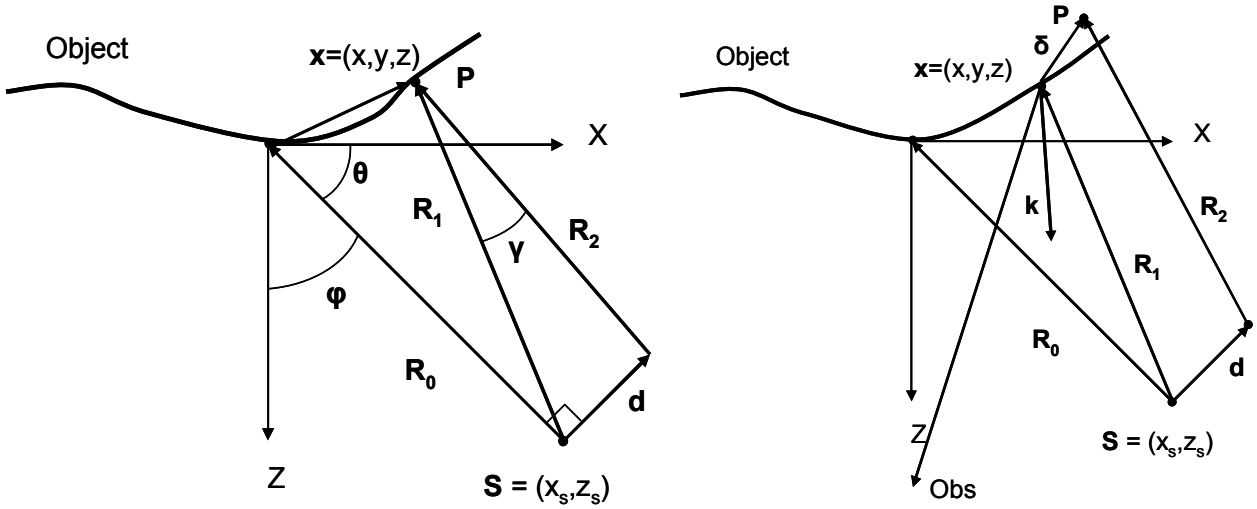

Figure 2. Problem geometry. Left diagram assumed without object motion. Right diagram shows a more detailed geometry for contouring analysis with object motion. Source location **S** and motion vector **d** are in X-Z plane, **d** is perpendicular to $\mathbf{R_0}$.

If, for the moment, we assume that the object is stationary between exposures (**δ** = 0), then the left side of Figure 2 describes the contouring situation. The source is translated by **d** between exposures, creating an optical path difference (OPD) of

$$\text{OPD} = N\lambda = \varphi / k = |\mathbf{R_2}| - |\mathbf{R_1}| \qquad \textbf{(1)}$$

By expanding $|\mathbf{R_2}| = |\mathbf{R_1} + \mathbf{d}|$ we see that

$$N\lambda \cong -\mathbf{d} \bullet \mathbf{R_1} \qquad \textbf{(2)}$$

Where $\hat{\mathbf{R}}_1 = \dfrac{\mathbf{R_1}}{|\mathbf{R_1}|}$ is a unit vector in the direction of $\mathbf{R_1}$. This requires the assumption that $|\mathbf{d}| << |\mathbf{R_1}|$, and introduces an error in OPD of order $\dfrac{|\mathbf{d}|^2}{|\mathbf{R_1}|}$. A similar assumption is made in ESPI deformation analysis, that $|\boldsymbol{\delta}| << |\mathbf{R_1}|$. However in ESPI, this is not nearly as strong an assumption, simply because $|\boldsymbol{\delta}|$, the deformation, tends to be on the order of microns, while $|\mathbf{d}|$, the motion imposed on the illumination source tends to be larger, perhaps hundreds of microns.

Wang, *et al* [4,5] point out that the solution for z can be simplified if the coordinate system is chosen so the source S and source translation vector **d** are in the X-Z plane, and **d** is perpendicular to $\mathbf{R_0}$, the vector from the source to the origin. (The latter causes the zero fringe to go through the origin, making possible the identification of absolute fringe order N). They derive a quadratic solution for the object topography z:

$$z = z_s + \frac{1}{2a}\left[-b \pm \sqrt{b^2 - 4ac}\right] \qquad \textbf{(3)}$$

Where

$$a = 1 - (N\lambda / w)^2$$
$$b = -2\tan\theta(x - x_s)$$
$$c = \tan^2\theta(x - x_s)^2 - (N\lambda / w)^2\left[(x - x_s)^2 + y^2\right]$$

And u and w are the components of $\mathbf{d} = (u\hat{x} + w\hat{z})$ and θ is the angle between $\mathbf{R_0}$ and the x-axis.

Choosing the correct root in equation 3 can be difficult. Wang [4] claims that the positive root can be selected whenever Nλ ≥ 0, but this is incomplete. The positive root is selected whenever the product of Nλ*w is less than zero (note that in Wang's "standard" configuration, depicted in Figure 2, w is less than zero). This extended criterion handles the situation where x_s is less than zero.

Other authors have suggested techniques for finding the OPD. Thalmann and Dandliker [1] correct for the effect of perspective viewing from a finite distance. Their final solution cannot be rendered as a closed form quadratic, but must be solved iteratively. Another method assumes that the distance to the illumination sources are sufficiently large relative to the object size that the illumination can be considered plane waves [3]. This requires the strongest assumptions and leads to the simplest analysis, but introduces unacceptably large errors for our particular geometry.

3. Simulations

We chose to simulate the Wang technique described above to better demonstrate the errors resulting from the various assumptions—especially the effect of object motion and our proposed corrections for this motion. The motivation for this work was measurement of both initial contour and electrostatically programmed deformation of a thin polyvinylidine fluoride (PVDF) film being developed for adaptive optics. The experimental geometry defined reasonable parameters and was used for our simulations. A square sample with sides of 87.2 mm was illuminated with a doubled YAG laser with λ = 0.532 μm, with an illumination distance **R** of 615 mm at an angle of 22 degrees from the normal to the sample. The sample was not flat, with an estimated deviation from a plane of a few mm. This was matched in the simulation by a surface with a few polynomial lumps in it..

We generated the actual path difference according to equation 1, and then used it in equation 3 to estimate the surface contour shown on the left of Figure 3. By subtracting the estimate from the actual surface, we can get the error estimate for the technique, as shown on the right of Figure 3. A planar error is introduced by the

asymmetry caused by assuming **d** is perpendicular to $\mathbf{R_0}$ and therefore cannot be perpendicular to $\mathbf{R_2}$ with **x** at the origin.

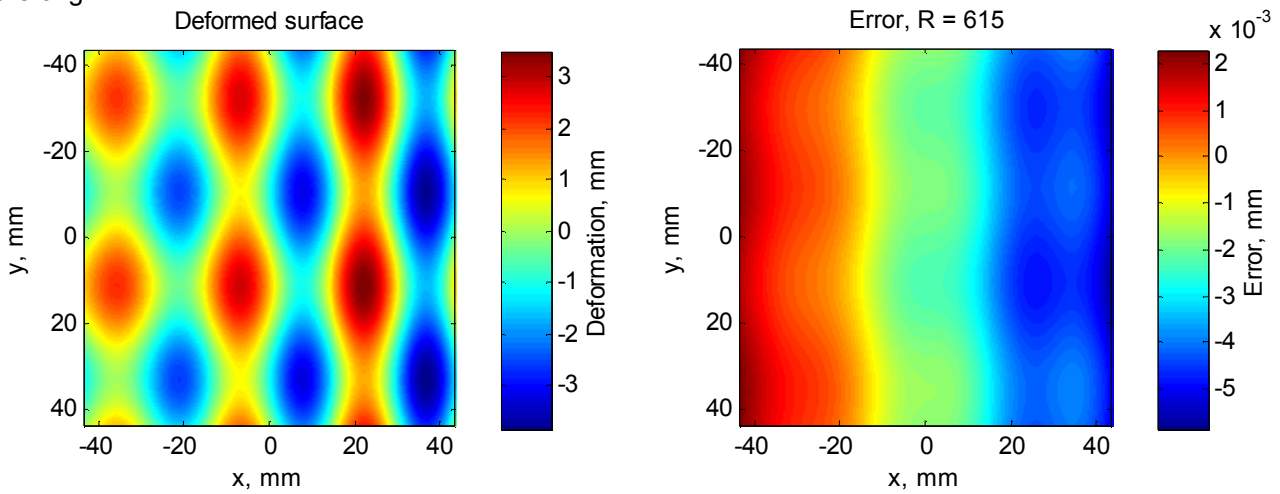

Figure 3. Simulated surface and resulting error surface using quadratic estimate.

If we fit a plane to the result, the error is reduced a bit as shown in left of Figure 4. In either case, the error is on the order of a few microns.

To verify that this is indeed algorithm error and not computational (roundoff) error, increasing R by an order of magnitude gives the much smaller error estimate shown in the right image in Figure 4.

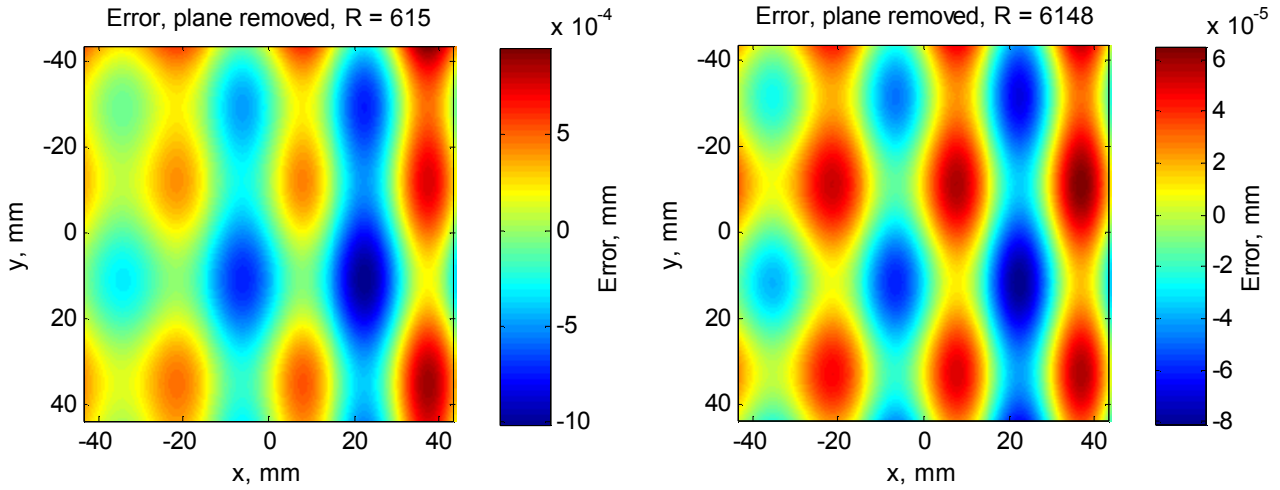

Figure 4. Error after plane removed from estimate and error with R increased by 10 times.

To estimate realistic accuracy in the presence of noise-induced phase errors, we can add a random phase error to the simulation. Adding a uniformly distributed path length error of λ/20 gives an estimated contour as shown in Figure 5, which has an error standard deviation of 0.3mm. This error, resulting from an admittedly conservative estimate of process noise, clearly dominates any error induced by the above estimates in algorithm derivation.

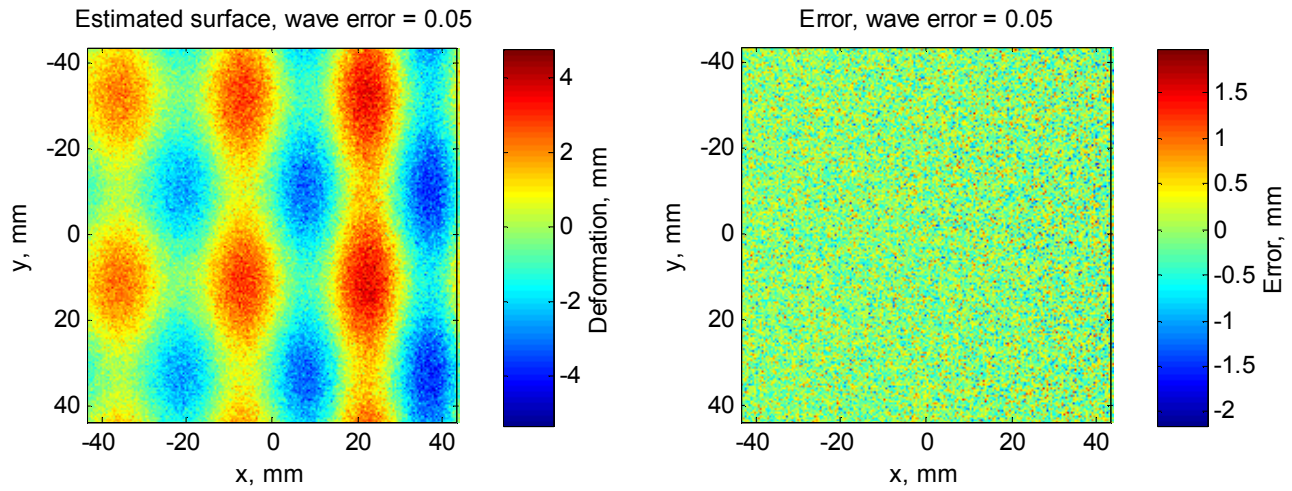

Figure 5. Surface estimate and error with λ/20 noise.

As mentioned in the introduction, one of the motivations for these simulations was to investigate the effects of sample motion during contouring measurement. Our original experimental goal was to measure both gross contour (possibly mm deviations from planar) and PVDF deformation (typically tens of microns for the drive levels we were using). Both of these measurements are out-of-plane (z) deviations, so we set up our ESPI system for out of plane deformation measurement (see Figure 1), and intended to make the contour measurement by moving the illumination source while keeping the drive voltage constant. Unfortunately, very small amounts of sample drift between contour datasets cause a large contour error, due to the sensitivity of the method to out-of-plane motion. To simulate this, we introduced a drift model. Equation 2 must be modified to include sample motion, as shown on the right of Figure 2:

$$N\lambda \cong -\mathbf{d} \bullet \mathbf{R}_1 + \mathbf{k} \bullet \boldsymbol{\delta} \qquad \textbf{(4)}$$

Since the sample is allegedly fixed at the edges, we chose to model drift by a parabolic out-of-plane deformation fixed at the corners. (Note that our algorithm assumes the zero fringe passes through the origin, which causes the z=0 point at the origin.) Even a tiny amount of drift, maximum of 0.2 μm in this example, causes an unacceptable error in contour as shown in Figure 6.

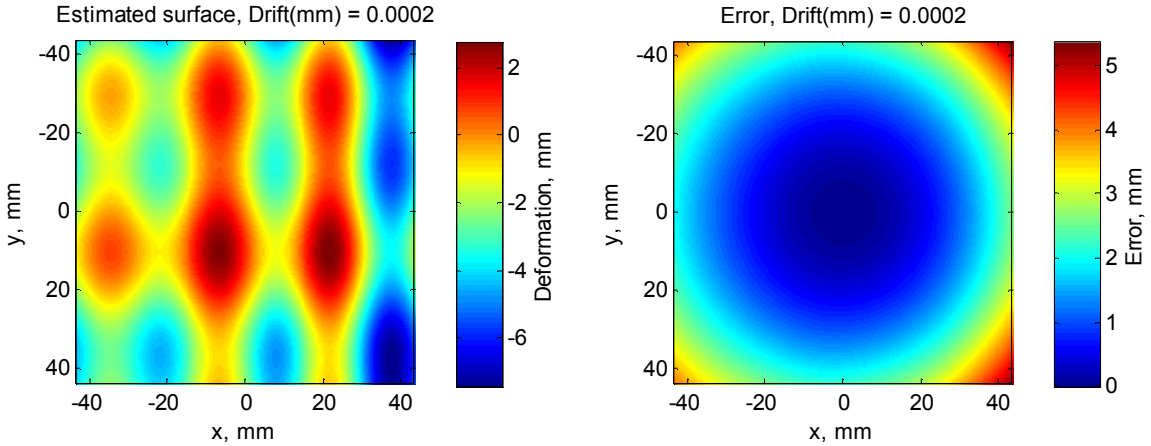

Figure 6. Contour result from simulation including drift and the resulting error surface.

4. Drift correction experiments

We suggest two possible methods to correct for sample drift; the first uses an assumption of constant drift during the experiment and the second arranges the system to be insensitive to out-of-plane motion. By

monitoring real-time ESPI fringes, and by measuring velocity of the sample center using a laser Doppler velocimeter (LDV), we determined that the sample drift was fairly constant over short times (a minute or so). To use the "constant drift" compensation method, three ESPI datasets are taken, moving the source from position 1 to position 2 (giving phase difference measurement 1), then back to position 1 (giving phase difference measurement 2). Taking the difference between the first and second phase difference measurements, we can subtract the $\mathbf{k}\cdot\boldsymbol{\delta}$ term from equation (4) and end up with $2N\lambda$ to use in our contouring algorithm, equation (3).

Of course, the contouring algorithm relies only on the total change in optical path length, as recorded by ESPI techniques. While a "reference beam" is necessary to make this measurement, it is not necessary that this reference be arranged to be sensitive to out-of-plane motion. If the reference beam is, instead, arranged to illuminate the object from a direction symmetrically opposed to the illumination beam, (in standard "in-plane" sensitivity mode with sensitivity vector **k** perpendicular to the Z axis), the ESPI system will be totally insensitive to out of plane motion. While this is less convenient for our particular application, it *should* solve the drift problem if our drift is primarily out-of-plane.

To experimentally verify these two methods, we generated a sample that is a bit more controllable than the PVDF film. A few strategically placed blows with a ball-peen hammer on a 1/16 inch sheet of aluminum created some lumps in the mm range to mimic our PVDF film. We used a commercial digital image correlation (DIC) system [6] to measure the contour of the aluminum sample as a comparison to our ESPI contouring method. The two results are shown in Figure 7.

Figure 7 compares the ESPI and DIC contours. While they agree within a few tens of microns around the lumps in the center, there are edge effects we have not identified—either filtering in the ESPI algorithms, edge effects in the DIC algorithms, or possibly both.

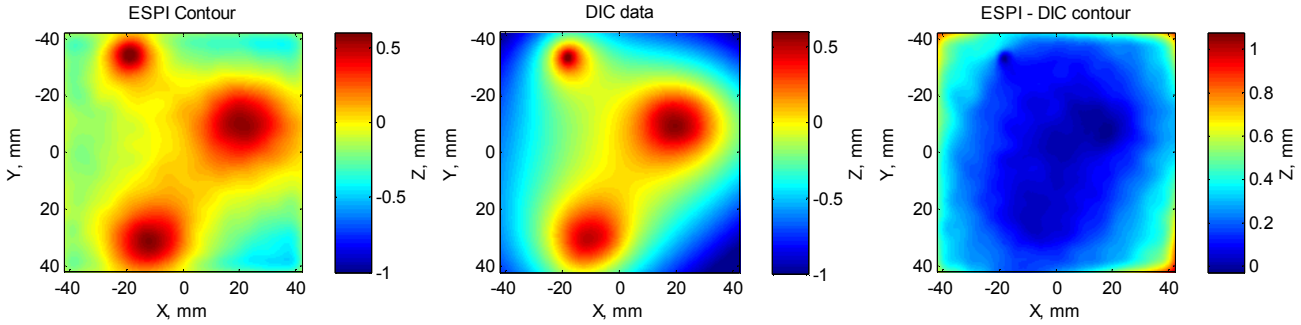

Figure 7. Aluminum plate comparison between ESPI contouring, DIC data and difference plot.

We introduced a drift by pushing on the back of the sample with a speaker coil driven by a constantly increasing current. The ramp was adjusted to provide a few fringes per second and was not calibrated, since only small constant drift was required. An ESPI deformation measurement taken with a few seconds between exposures shows the drift deformation in Figure 8. Figure 8 also shows the result of contouring with sample drift, without compensation. A few microns of drift cause many mm of contour error.

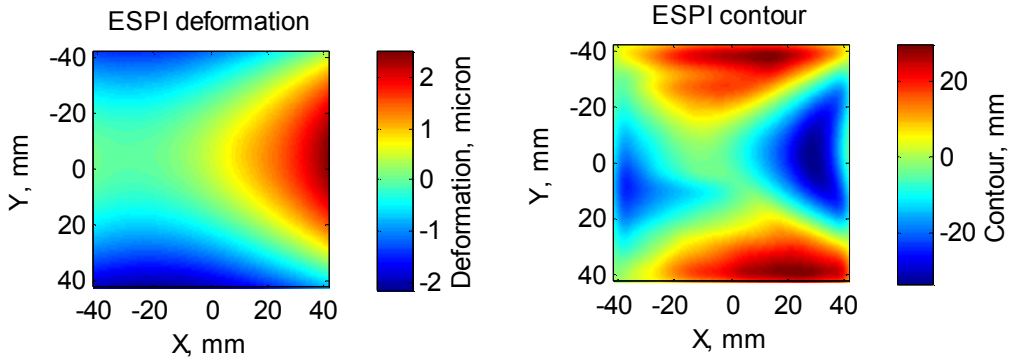

Figure 8. Drift deformation shape (left), contour data with drift uncompensated (right)

Figures 9 and 10 compare the results of the two drift compensation techniques applied to the cal plate with constant drift.

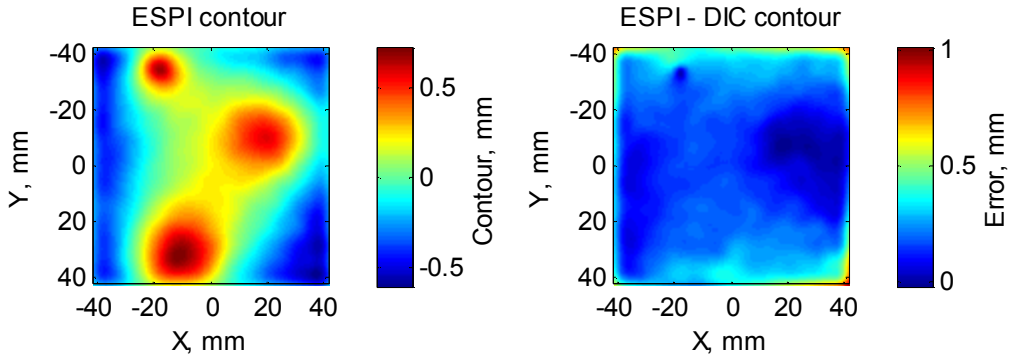

Figure 9. Contouring with constant drift compensation (left) and error (difference between ESPI contour and DIC contour).

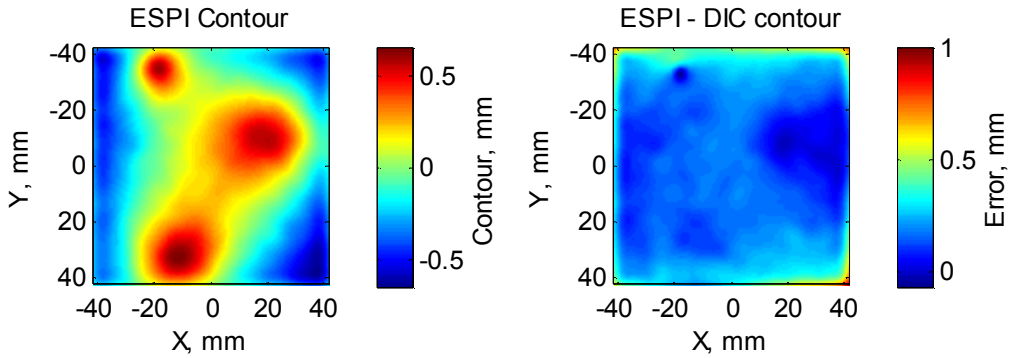

Figure 10. Contouring with in-plane drift insensitive configuration (left) and error (difference between ESPI contour and DIC contour).

Using the PVDF film for contouring, some measurements of the repeatability were done by making four independent measurements and then calculating, on a pixel-by-pixel basis the mean contour and the RMS error. Figure 11 shows the results with the out-of-plane sensitivity vector using the two-measurement compensation. Figure 12 shows results from 4 datasets where the sensitivity vector is in-plane, which we thought would be the "best" results. The RMS image gives an indication of how consistent the results are, but of course we don't know the "correct" answer in this case so this is not an error image.

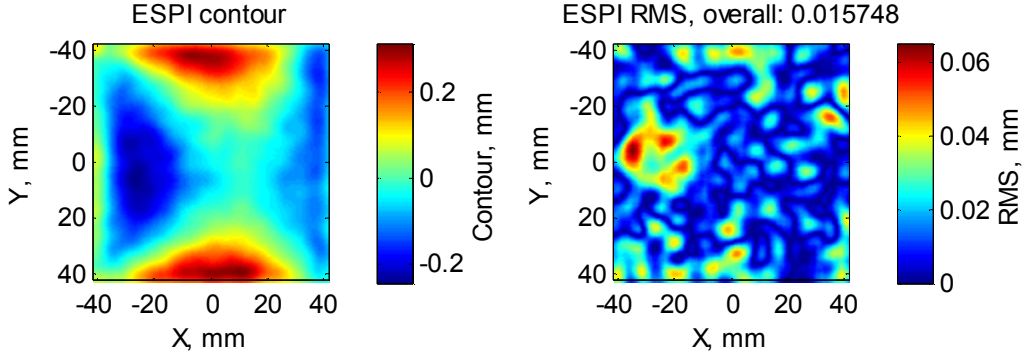

Figure 11. Two-measurement drift compensated results of PVDF film and RMS error.

The two-measurement method actually shows a bit better consistency than the in-plane sensitivity vector method. (This could be due to the fact that this measurement actually relies on twice as many independent measurements as the in-plane method, thus introducing more averaging). In either case, we see a consistency of a few tens of microns—clearly the absolute error is no *less* than this, hopefully it is not much greater. RMS values calculated with no compensation are on the same order and clearly demonstrate that the RMS error is not an indication of accuracy, but repeatability.

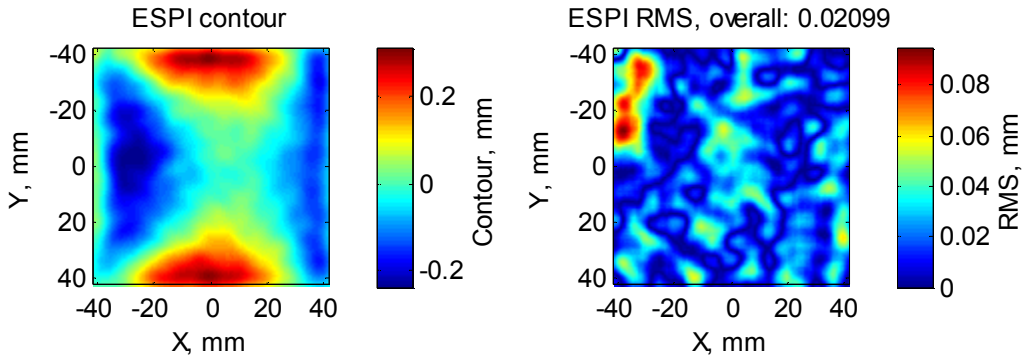

Figure 12. PVDF contour measured with insensitive alignment and RMS error.

5. Conclusions

We have investigated some assumptions inherent in various ESPI contouring algorithms, and the error magnitudes resulting from these assumptions. We conclude that, for practical geometries (object a few tens of mm in size, optical distances a few hundred mm) the quadratic algorithm presented by Wang, *et al* provides accuracies to a tenth of a percent, *provided the object is totally stationary during the data acquisition*. In this case, errors introduced by even modest amounts of phase noise are much greater than the errors caused by the assumptions in the algorithm derivations. We pointed out that object motion can be a serious problem in these measurements, since the contour distance is highly sensitive to changes in optical path length. We presented two techniques to compensate for object motion, if the motion is relatively constant over the period of data acquisition and validation experiments of these techniques.

Acknowledgements

Sandia is a multiprogram laboratory operated by Sandia Corporation, a Lockheed Martin Company, for the United States Department of Energy under contract DE-AC04-94AL85000.

References

[1] R Thalmann and R. Dändliker, Holographic contouring using electronic phase measurement, Optical Engineering 24(6) (Nov/Dec 1985), 930-935

[2] C. Joenathan, B. Pfister and H. J. Tiziani, "Contouring by electronic speckle pattern interferometry employing dual beam illumination", AO **29**(13), 1905-1912 (May 1990).

[3] R. Rodriguez-Vera, D. Kerr, and F. Mendoza-Santoyo, "Electronic speckle contouring", JOSA A **9**(11), 2000-2006 (Nov 1992).

[4] L. S. Wang, K. Jambunathan, B. N. Dobbins and X. P. Wu, Fibre optic shape measurement system using phase stepping speckle pattern interferometry, SPIE vol 2088 (Feb 1993), 104-110.

[5] L. S. Wang, K. Jambunathan and B. N. Dobbins, Measurement of 3D surface shape and deformations using phase stepping speckle interferometry, OE vol 35(8), Aug 1996, pp2333-2340.

[6] DIC from Correlates Solutions http://www.correlatedsolutions.com